

Velocity measurement of particulate flow in microfluidic channels using single point confocal fluorescence detection

Joshua B. Edel, Elisabeth K. Hill and Andrew J. de Mello*

AstraZeneca/SmithKline Beecham Centre for Analytical Sciences, Imperial College of Science, Technology and Medicine, Department of Chemistry, South Kensington, London, UK SW7 2AY. E-mail: a.demello@ic.ac.uk

Received 23rd July 2001, Accepted 31st August 2001

First published as an Advance Article on the web 17th October 2001

This article presents a non-invasive, optical technique for measuring particulate flow within microfluidic channels. Confocal fluorescence detection is used to probe single fluorescently labeled microspheres (0.93 μm diameter) passing through a focused laser beam at a variety of flow rates (50 nL min^{-1} –8 $\mu\text{L min}^{-1}$). Simple statistical methods are subsequently used to investigate the resulting fluorescence bursts and generate velocity data for the flowing particles. Fluid manipulation is achieved by hydrodynamically pumping fluid through microchannels (150 μm wide and 50 μm deep) structured in a polydimethylsiloxane (PDMS) substrate. The mean fluorescence burst frequency is shown to be directly proportional to flow speed. Furthermore, the Poisson recurrence time and width of recovered autocorrelation curves is demonstrated to be inversely proportional to flow speed. The component-based confocal fluorescence detection system is simple and can be applied to a diversity of planar chip systems. In addition, velocity measurement only involves interrogation of the fluidic system at a single point along the flow stream, as opposed to more normal multiple-point measurements.

Introduction

The study of solid particles within flowing streams is of great interest and importance in biological and industrial systems.¹ Examples include the measurement of the effect of various interventions on regional blood flow,² particulate flow in smokestacks and the study of fuel injection in combustion engines. Furthermore, particles have also been used to monitor bulk flow in micro structures³ as well as simulating the inhalation of airborne particles.⁴

Key requirements when measuring particulate velocities include the need for a sensitive, non-invasive detection protocol as well as the ability to continuously monitor a given system. This is important, since invasive methods, such as placing a probe in the flow, cause disruption and induce an error in the velocity measurements. Fluorescence methods are inherently sensitive, non-invasive and selective and therefore are well suited for use in velocimetry measurements. A common technique usually applied in particle velocimetry relies on the fundamentals of the Doppler shift. Doppler shift is a change of the wavelength of a wave, due to the difference in velocity between the source of the wave and the observer. In laser Doppler techniques light incident on a moving object is scattered and frequency shifted according to standard physical models. Unfortunately, laser Doppler techniques involve the use of complicated and expensive instrumentation, and require that the laser beam, optics, and detector must all be precisely aligned. Particle Image Velocimetry (PIV) is another well-established technique used in both macroscopic and microscopic flow systems to measure fluid velocity fields. The PIV technique works by calculating the displacement of many small "tracer" particles injected into the fluid being measured. The particles are assumed to follow the fluid motion as well as not significantly changing the fluid properties such as density, volume and viscosity. Conventionally, a pulsed laser is used to illuminate and fix the motion of the particles while a CCD camera images the particles. After a defined time-delay a second image of the particles is recorded. A correlation algorithm is applied to the pair of images to yield the mean

displacement of the particles between the two exposures. Division of the displacement by the time-delay returns the velocity field of the fluid. PIV has been used to investigate a wide variety of fluid flow fields in systems including microchannels and micro-nozzles.^{5,6} In addition, Manz and co-workers recently used Shah Convolution Fourier Transform Detection (SCOFT) for velocity measurements of fluorescent microspheres within microfluidic channels.¹ Their approach used a novel convolution-detection method to convert multiple-point detection, time-domain electropherograms to frequency-domain plots.

Over the past several years, high sensitivity detection has become increasingly important in biological and chemical analysis. This is primarily due to a general need for rapid, on-line measurements at low concentrations. Recently, techniques have been developed to demonstrate and utilize ultrasensitive fluorescence detection at the individual molecular level.^{7,8,9} Single-molecule detection (SMD) in solution has been reported for a number of fluorophores and applied to several regimes. SMD approaches are particularly interesting since they afford the evaluation of individual molecular behaviour rather than ensemble measurement.¹⁰ A comprehensive review of advances in the field of SMD can be found elsewhere.¹¹

Keller and co-workers first suggested the use of laser induced fluorescence (LIF) for single-molecule detection in a flowing sample.¹² Examples of LIF include fluid velocity measurements in a biofilm system using confocal scanning laser microscopy.¹³ Another particle imaging method involves the illuminating of a two-dimensional slice of refractive index matched model of a porous medium with a planar laser beam. Time-sequenced photographs provide quantitative information about the velocity of the flowing liquid.¹⁴ Rigler *et al.* first reported the use of a confocal microscope coupled with fluorescence correlation spectroscopy (FCS)¹⁵ to detect the translational diffusion of a single Rhodamine 6G molecule in water. The volume interrogated by the laser beam using confocal detection is typically in the femtolitre range (10^{-15} L). In confocal fluorescence the low detection volume greatly reduces the amount of sample needed for analysis over conventional bulk detection methods. When a

dilute solution (analyte) is used with a concentration of approximately 10^{-9} M there is on average less than one fluorescent molecule or particle resident in the probe volume.¹⁶

Recently, the application of planar chip microfluidic technology to analytical processing has been demonstrated to afford advantages in terms of improved efficiency with respect to sample size, response time, cost, throughput and automation. Indeed, microfluidic devices have been successfully applied in the areas of DNA analysis, separation science, DNA amplification, immunoassays, small molecule synthesis and cell manipulation.^{17–20} In general, real challenges for detection arise due to the scale of miniaturized devices and the associated sample volumes (nL–pL).¹⁸ The small probe volumes associated with confocal detection are insensitive to sample downsizing and thus provide an interesting route to high-sensitivity on-chip detection. For example, Mathies and co-workers²¹ have used single molecule fluorescence burst counting techniques to detect DNA separations performed within microfabricated capillary electrophoresis chips. Furthermore, Effenhauser *et al.* have demonstrated single-molecule detection of YOYO-1 intercalated λ DNA strands in a PDMS chip.²² These and other studies highlight a trend towards highly efficient single molecule detection in microstructures for DNA sequencing applications.²³ More recently, Rigler and co-workers demonstrated high-spatial resolution flow profiling in microchannels using FCS. By scanning microchannels with a diffraction-limited laser focus the authors report the detection of single tetramethylrhodamine labeled biomolecules at various locations within the microchannel. Subsequent autocorrelation analysis of the resulting burst scans demonstrated parabolic flow in both dimensions (*i.e.* Poiseuille laminar flow).²⁴

In this article we present experimental studies relating to the detection of solid microspheres flowing through microchannels. A confocal fluorescence detection approach is used to probe single microspheres passing through a focused laser beam at a variety of flow rates. Simple statistical methods are subsequently used to investigate the resulting fluorescence bursts and generate velocity data for hydrodynamically flowing particles.

Experimental

Apparatus

Precise details of the experimental system are described elsewhere.¹⁶ Briefly, the excitation source used in all experiments is a CW air-cooled argon ion laser operating in light control mode at 488 nm and 7.0 mW (Omnichrome; Melles Griot, Cambridge, UK). Beamsteering optics direct the light into the confocal system, with glass neutral density filters (0.2–4 absorbance units) attenuating the laser intensity as required (Newport Ltd., Newbury, UK). In addition, the laser beam is spatially filtered (5-axis compact filter; Newport Ltd.) in order to ensure a near-Gaussian intensity profile.

A dichroic mirror (505DRLP02; Omega Optical, Brattleboro, VT, US) is oriented at 45° to reflect 488 nm radiation and so define a vertical axis, normal to the surface of the optical table. An infinity corrected, high numerical aperture (NA) microscope objective (Fluar 100 \times /1.3 NA, oil immersion; Carl Zeiss Ltd., Welwyn Garden City, UK) brings the light to a tight focus within the sample chamber. The collimated laser beam has a $1/e^2$ diameter of 2.5 mm. This width is selected to nearly fill the back of the microscope objective, and so yield a beam focus estimated to be close to the diffraction limit. The beam diameter (d) is given by eqn. (1)

$$d = \frac{1.27\lambda f}{nD} \quad (1)$$

where D is the incident diameter of the laser radiation at the objective, n is the refractive index of the focusing media, f is the focal length of the objective and λ is the lasing wavelength. The focused laser spot defines an approximate probe volume of 0.42 fL.

Poly(dimethylsiloxane) (PDMS) microfluidic chips are used and fabricated in-house using standard photolithography and etching techniques.²⁵ The resulting microstructured channels in the PDMS substrates are 150 μm wide and approximately 50 μm deep. A simple ‘double-Y’ channel pattern (Fig. 1) was designed to allow flexibility in the number of inlets and outlets. However, in all current studies, one inlet and three outlets were used. The structured substrates are approximately 1 cm^2 and 5 mm thick. The PDMS substrate was covered with a 18×18 mm glass cover slip (grade 0; BDH Merck, Poole, Dorset, UK) having a thickness of less than 130 μm (the maximum working distance of the microscope objective is 150 μm). A reversible seal is formed between the glass and PDMS. This allows for facile cleaning of the microchip when needed. Cleaning of the PDMS surface was typically performed by sonicating the substrate in ethanol followed by rinsing in deionized water. Hole reservoirs were bored in the PDMS and 3 cm long pieces of 75 id/150 od capillary (Polymicro Technologies, Phoenix, AZ, USA) was inserted into the reservoir holes. The capillaries were secured in each port with Loctite Prism 406 cyanoacrylate adhesive (RS Components, Corby, UK). The microchip is placed on a translation stage and appropriately aligned under the microscope objective. A syringe pump (Harvard Apparatus, Cambridge, MA, USA) is used to deliver solutions at various flow rates from either a 500 μL or 50 μL gastight syringe into the capillary tubing. Typical flow rates ranged from 0.05–8 $\mu\text{L min}^{-1}$.

Fluorescence emitted by the sample is collected by the same high NA objective and transmitted through the dichroic mirror. An emission filter (515EFLP; Omega Optical, Brattleboro, VT, USA) removes any residual excitation light. A plano-convex lens (+50.2F; Newport Ltd., Newbury, UK) focuses the fluorescence onto a precision pinhole (25 μm ; Melles Griot, Cambridge, UK) placed immediately in front of the detector. The pinhole is positioned in the confocal plane of the microscope objective.

The detector is a silicon avalanche photodiode operating in single-photon counting mode (SPCM-AQR-141; EG&G Canada, Vaudreuil, Quebec, Canada). The dark count rate on average was well below 60 Hz. The precision pinhole and detector are mounted on an XY translation stage to allow for fine adjustment of the incoming radiation. The electronic signal from the detector is coupled to a multi channel scalar (MCS-PCI; EG&G Canada, Vaudreuil, Quebec, Canada), running on a

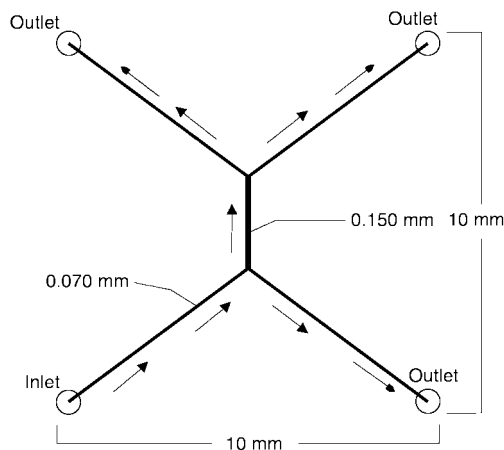


Fig. 1 Schematic of ‘Double-Y’ PDMS microchip used for all analyses. The detection volume was positioned at a point midway along the wide (150 μm) channel.

Pentium PC. The spectra recorded were converted into an ASCII file and transported into Excel© as well as several C++ programs (code written in-house) in order to perform appropriate statistical analysis on the outputted data.

Materials

Fluorescent microbeads (yellow/green fluospheres®, Molecular Probes; Eugene, OR, USA) having a mean diameter of 0.93 μm were used for all experiments. Absorption and emission maxima were 505 nm and 515 nm respectively. The beads were sonicated for 10 min immediately before use to ensure good dispersion. A working solution of approximately 2.3×10^7 beads per mL was used (effective concentration of 10 $\mu\text{g mL}^{-1}$). This is equivalent to a 2000 fold dilution of the stock solution. All dilutions were performed in TBE (tris–borate–EDTA) buffer. The TBE buffer was prepared at 0.1 \times concentration [8.9 mM each of tris(methoxy)aminomethane and boric acid, 0.2 mM in ethylenediaminetetraacetic acid; prepared from a solid TBE mixture (Fluka, Poole, Dorset, UK)] in a minimum of 18 M Ω deionized water (water purification system, Elga Ltd., Bucks, UK).

Results and discussion

Fig. 2 shows examples of fluorescent bursts scans from 0.93 μm fluospheres at volumetric flow rates of 1000, 200 and 50 nL min^{-1} . Average signal intensities, using a dwell time of 1 ms, were typically of the order of 300 counts. It can be seen in all scans that burst heights vary significantly in magnitude. This is primarily caused by the range of possible particle trajectories through the probe volume and is observed due to the diffraction-limited focus of the laser beam being approximately 150 times smaller than the channel width of the microfluidic device (a reduction in the channel width would result in a more uniform signal intensity and burst width). A signal to noise ratio as high as 200 is typically observed for any given flow rate. An average background signal intensity of ~ 4 counts per bin for flow rates ranging from 50–8000 nL min^{-1} remained approximately constant throughout each acquisition. The background threshold was therefore set to 10 counts per bin for all experiments as was predicted by a Poissonian analysis. Variation of the laser power (between 0.5 and 7 μW) resulted in no significant change in signal to noise ratios.

Expanded portions of the burst scans in Fig. 2 clearly show the low-level background signal as well as the variation in burst frequency and burst width. Analysis of the dwell time *versus* burst width data yields information relating to the time spent by individual fluospheres in the probe volume. For example for a flow rate of 1000 nL min^{-1} residence times were calculated as

a function of dwell time (between 10 and 800 μs). It is at these dwell times in which single particle bursts are observed (at higher dwell times each burst is due to the presence of more than one particle). This analysis yielded an average burst width of 1.38 ms with excellent precision. It should also be noted that in these studies much higher signal to noise ratios are obtained when compared to single molecule detection. This is due to the fact that each fluosphere particle contains approximately 1.0×10^7 fluorescein equivalents.

Three methods of analysis were used to characterize single particle bursts at various flow rates. The first, Autocorrelation analysis, has been shown to be an extremely sensitive method for detecting the presence of fluorescence bursts in single molecule and single particle experiments.^{26,27,28} Autocorrelation analysis essentially measures the average of a fluctuating signal as opposed to the mean spectral intensity. The standard autocorrelation function, $G(\tau)$, is defined in eqn. (2).

$$G(\tau) = \sum_{t=0}^{N-1} g(t)g(t+\tau) \quad (2)$$

Here $g(t)$ is the total number of counts during the time interval $(t, t + \Delta t)$, $g(t + \tau)$ is the number of counts detected in an interval of Δt at a later time $t + \tau$, and N is the total number of time intervals in the dataset. In a flowing system the autocorrelation function depends on the average flow time through the probe volume t_{flow} . A theoretical fit to the function can be described according to,

$$G(\tau) = 1 + \frac{1}{N} A \exp\left\{\left(\frac{\tau}{\tau_{\text{flow}}}\right)^2 A\right\} \quad (3)$$

$$A = \left(1 + \frac{\tau}{\tau_d}\right)^{-1} \left(1 + \left(\frac{\omega}{z}\right)^2 \frac{\tau}{\tau_d}\right)$$

where τ_d is the characteristic diffusion time, N is the mean probe volume occupancy, ω defines the laser beam waist radius and $2z$ defines the probe depth.²⁶ Eqn. (3) clearly shows that as the flow velocity is increased the full width half maximum (FWHM) of the autocorrelation function decreases. Fig. 3(A) shows normalized autocorrelation curves for two different bulk volumetric flow velocities. As expected at the higher flow rate (1000 nL min^{-1}), the FWHM is smaller when compared to that of the lower flow velocity (200 nL min^{-1}). The autocorrelation curves were calculated using a C++ program as opposed to using a hard-wired digital autocorrelator.

Another method for the quantitative examination of fluorescent bursts at various flow rates utilizes the analysis of Poisson statistics. Burst interval distributions are predicted to follow a Poissonian model, in which peak separation frequencies adopt an exponential form.^{28,29} The probability (or the number of

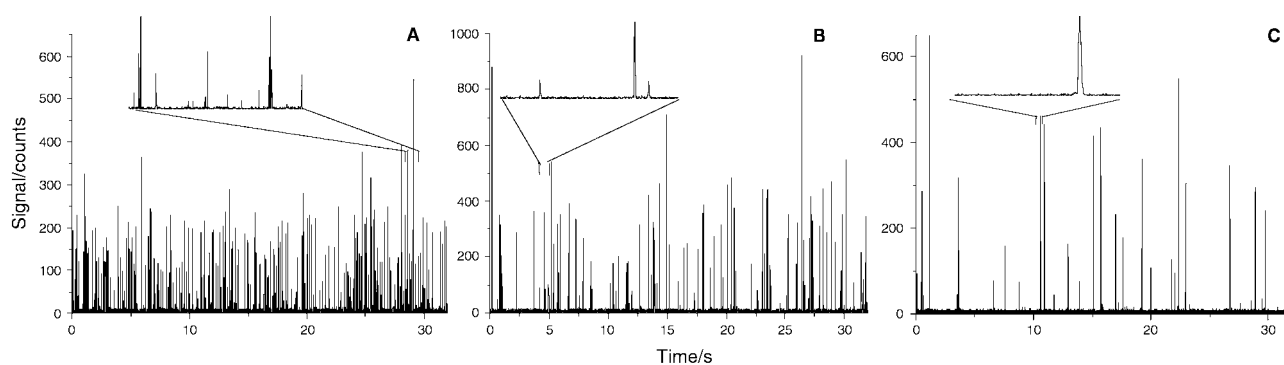


Fig. 2 Representative single-particle fluorescence burst scans of 0.93 μm fluospheres in a TBE (tris–borate–EDTA) buffer (effective concentration of 10 $\mu\text{g mL}^{-1}$) at a variety of flow rates: **A** 1000 nL min^{-1} , **B** 50 nL min^{-1} and **C** 200 nL min^{-1} . Insets show expanded burst details. Acquisition time: 1 ms per data point.

times N) of a single particle event recurring after an interval Δt is given by eqn. (4).

$$N(\Delta t) = \lambda \exp(-\beta \Delta t) \quad (4)$$

where λ is a proportionality constant and β is a characteristic frequency at which single molecule events occur. The recurrence time τ_R can then be simply defined as,

$$\tau_R = \frac{1}{\beta} \quad (5)$$

Eqn. (4) simply states that longer intervals between photon bursts are less probable than shorter intervals at a given flow rate. Furthermore, the recurrence time reflects a combination of factors that control mobility, probe volume occupancy or other

parameters in the single molecule regime. Consequently, τ_R is inversely proportional to concentration, flow rate or solvent viscosity in a range of systems. Fig. 3(B) shows frequency $N(\Delta t)$ versus time plots for two flow rates. A least squares fit to a single exponential function yields values of $\tau_R = 91$ ms for a volumetric flow rate of 200 nL min^{-1} and $\tau_R = 58$ ms for a volumetric flow rate of 1000 nL min^{-1} .

The final method applied to the analysis of flow velocities within microchannels simply utilizes the total fluorescent bursts counted at a given flow rate. The relationship between burst frequency and flow rates will be discussed in detail in the following paragraph. Bursts are located in the same manner as in the Poisson analysis. That is, a photon burst is defined by a fluorescent signal greater than a given threshold value. $C_{\text{threshold}} = \mu + 3(\mu)^{0.5}$, where μ is a single parameter relating to the mean and variance of a Poisson distribution.

As noted, typical burst recurrence times should be inversely proportional to the flow rate. Therefore, a linear relationship will exist between the burst recurrence rate and the flow rate for a given sample concentration and cross-sectional area of the micro-channel. Figs. 4(A) and (B) show plots of frequency *versus* flow rate and the reciprocal of the recurrence time *versus* flow rate respectively (each point is the average of 6.4×10^4 bins of data). In both cases a linear relationship is observed when the data are plotted on a log-log scale. The R^2 values, for a least squares linear fit, in both cases are above 0.98. It is interesting to note that in neither case does the extrapolated value at a flow rate of 0 nL min^{-1} yield a frequency of 0 counts or a $1/\tau_R = 0$. This is due to natural diffusive behaviour of the fluorophores through the excitation cavity of the probe volume. Data points below 50 nL min^{-1} were not obtained due to restrictions on the attainable flow rates with the pumping source. At flow rates above 2000 nL min^{-1} , although not obvious from a log-log plot, there is a slight gradual trend for the burst frequencies to deviate from the regression line. This is due to the fact that a proportion of bursts are not fully resolved on the timescale of the measurement. Increasing the chip capillary cross-section would minimize this effect, although the burst detection frequency would be reduced.

As previously mentioned there are clear variations in the width of the autocorrelation curve as a function of volumetric flow rate. Primarily, the width of a curve narrows with increasing flow speed. The reduced curve width is related to the reduced residence time of the particle in the probe volume, which is consistent with increased particular velocities. Fig. 4(C) plots the inverse of the FWHM value against the flow rate for a series of autocorrelation functions. A similar linear relationship is observed when comparing the data obtained to the plots in Figs. 4(A) and (B). All data plotted, for a given flow rate, are an accumulation of 6.4×10^4 bins of data at dwell times ranging from 0.8–2 ms. The acquisition time per data point therefore ranges between 52 and 128 s. It would be expected from Poissonian counting statistics that increasing the

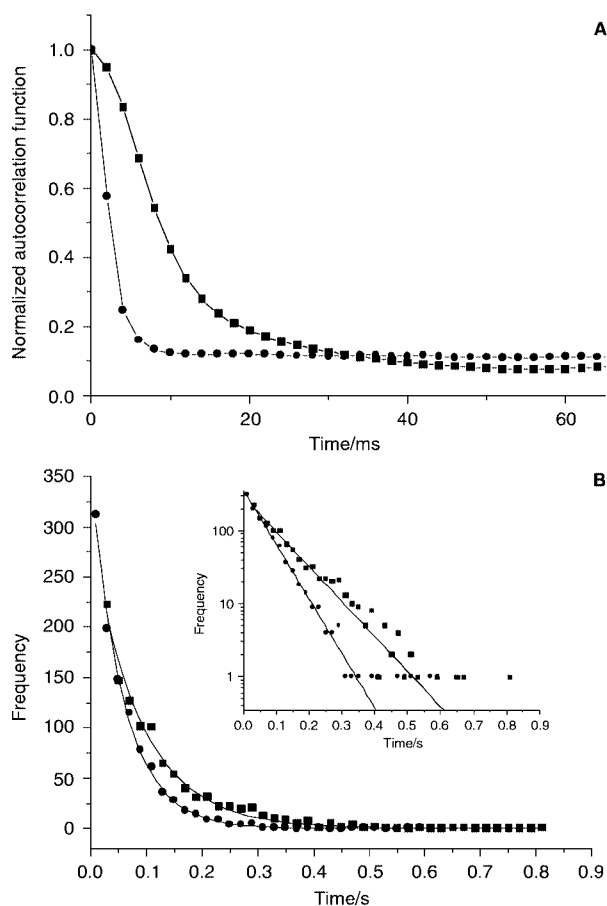


Fig. 3 Statistical analysis of single-particle fluorescence burst scans of $0.93 \mu\text{m}$ fluospheres at flow rates of 200 nL min^{-1} (squares) and 1000 nL min^{-1} (circles): **A**, experimental autocorrelation functions; **B**, burst interval distribution calculated from experimental data, with a least squares fit to a single exponential function (solid line).

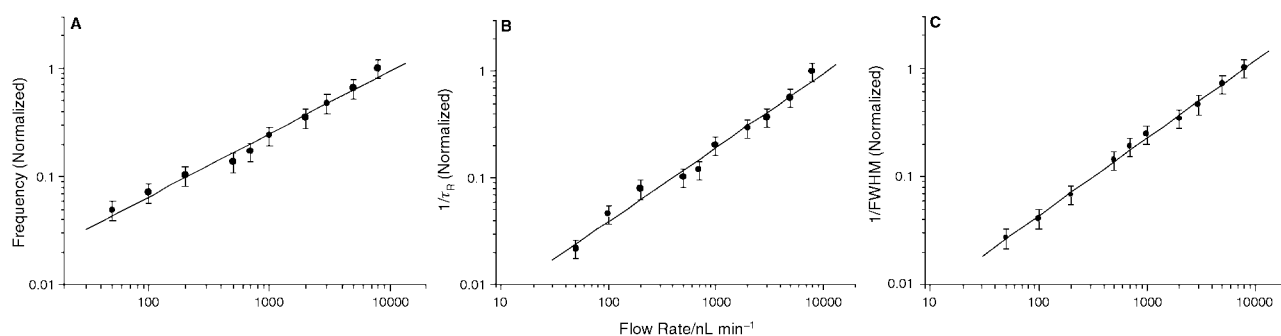


Fig. 4 **A**, Variation of the normalized burst frequency as a function of flow rate (gradient = 0.72). **B**, Variation of burst recurrence time as a function of flow rate (gradient = 0.75). **C**, $1/\text{FWHM}$ value of autocorrelation curve as a function of flow rate (gradient = 0.75). Experimental conditions: $0.93 \mu\text{m}$ fluospheres in a TBE (tris–borate–EDTA) buffer (effective concentration of $10 \mu\text{g mL}^{-1}$). Acquisition time: 1 ms per data point.

acquisition time would result in a greater number of counts being detected and thus a reduction in the standard deviation. As a result a higher precision, in the linear least squares fit, would be expected.

Discussion

The linear relationships observed in Figs. 4(A–C) demonstrate the application of confocal fluorescence detection as an indirect and non-invasive method for flow velocity determination within microfluidic channels. The mean burst frequency is shown to be directly proportional to particle velocity, and both the Poisson recurrence time and the autocorrelation FWHM are inversely proportional to flow speed. From the linear relationships observed in Figs. 4(A–C) the plot of $1/\text{FWHM}$ versus flow rates yields the best least-squares fit ($R^2 = 0.998$) and thus appears to be the best method for extracting flow velocities. This is consistent with observations made in previous studies.^{24,26} The recurrence time and frequency plots in Figs. 4(A) and (B) have reduced R^2 values of 0.982 and 0.985 respectively. A possible explanation for this reduced precision stems from the fact that in order to obtain frequency and recurrence times the background signal must be manually removed from the raw data resulting in a slightly larger error. Conversely, the FWHM is calculated by simply operating on the raw data to generate the autocorrelation curve. However, measurement of both recurrence times and burst frequencies provide alternative and facile methods of flow velocity determination within microfluidic channels. Furthermore, it should be noted that we calibrate particulate motion in terms of volumetric flow rate and not in terms of linear flow velocities. This is due to a number of reasons. First, actual particulate velocities are dependent on channel dimensions within a given fluidic network. Since these vary within the structure presented (and indeed will normally vary in any microfluidic circuit) volumetric flow rates provide the most suitable measure of particulate motion. Furthermore, calculation of a simple mean linear flow velocity would be misleading for the current studies, since parabolic flow profiles are generated by hydrodynamic pumping methods, and there is also an uncertainty in the exact location of the probe volume within the channel.²⁴

On a practical level, the confocal approach is appealing since it involves interrogation of the fluidic system at only a single point, with particulate flow velocities being determined from recurrence, frequency, and autocorrelation data. The component-based confocal fluorescence detection system is simple, inexpensive and can be applied to a diversity of planar chip systems without any modification of the chip construct (*e.g.* the deposition of fixed slit arrays necessary in SCOFI methods). As expected, the small probe volumes associated with confocal fluorescence methods are shown to be insensitive to sample downsizing and high sensitivity detection is achieved within microfluidic channels.

Although, the studies reported herein relate to the measurement of micron size particle velocities within fluid flow streams, the method is equally applicable to the determination of molecular velocities. We are currently assessing the described approach to the study of DNA within microfluidic systems. Initial results demonstrate similar correlations between flow rates and burst frequency, molecular recurrence time and autocorrelation FWHM above the diffusion-controlled limit. At very low volumetric flow rates ($< 1 \text{ nL min}^{-1}$) these dependencies are lost due to the fact that molecular diffusion begins to dominate motion.³⁰ In addition, flow velocity measurements of this kind may prove useful in applications such as high-

throughput screening and cellular assays. It is noted that although the small confocal probe volumes currently used reduce the efficiency with which single molecules can be counted, the laminar flow environment encountered within most microfluidic systems can be used to confine sample streams to more localized regions surrounding the probe volume.¹⁸

Acknowledgements

The authors would like to acknowledge EPSRC UK for financial support. Furthermore, J.E. acknowledges the receipt of an Overseas Research Studentship from the UK Government and E.H. is grateful to SmithKline Beecham Pharmaceuticals for an EPSRC CASE studentship.

References

- 1 Y. Kwok, N. T. Jeffery and A. Manz, *Anal. Chem.*, 2001, **73**, 1748.
- 2 R. L. Conhaim and L. A. Rodenkirch, *Am. J. Physiol.*, 1996, **271**, H996.
- 3 S. L. R. Barker, D. Ross, M. J. Tarlov, M. Gaitan and L. E. Locascio, *Anal. Chem.*, 2000, **72**, 5925.
- 4 H. T. Robertson, R. W. Glenny, D. Stanford, L. M. McInnes, D. L. Lucht and D. J. Covert, *Appl. Physiol.*, 1997, **82**, 943.
- 5 J. G. Santiago, S. T. Wereley, C. D. Meinhart, D. J. Beebe and R. J. Adrian, *Experiments in Fluids*, 1998, **25**, 316.
- 6 S. Devasenathipathy, J. C. Mikkelsen and J. G. Santiago, presented at the 219th ACS National Meeting, March 26–30, 2000, San Francisco.
- 7 S. Nie, D. T. Chiu and R. N. Zare, *Anal. Chem.*, 1995, **67**, 2849.
- 8 B. B. Haab and R. A. Mathies, *Anal. Chem.*, 1995, **67**, 3253.
- 9 E. B. Shera, N. K. Seitzinger, L. M. Davis, R. A. Keller and S. A. Soper, *Chem. Phys. Lett.*, 1990, **174**, 553.
- 10 R. Erdmann, J. Enderlein and C. Seidel, *Bioimaging*, 1998, **6**, 1.
- 11 W. P. Ambrose, P. M. Goodwin, J. H. Jett, A. van Orden, J. H. Werner and R. A. Keller, *Chem. Rev.*, 1999, **99**, 2929.
- 12 N. J. Dovichi, J. C. Martin, J. H. Jett and R. A. Keller, *Science*, 1982, **219**, 845.
- 13 L. Stoodley, D. Debeer and Z. Lewandowski, *Appl. Environ. Microbiol.*, 1994, **60**, 2711.
- 14 M. A. Northrup, T. J. Kulp and S. M. Angel, *Anal. Chim. Acta*, 1991, **255**, 275.
- 15 R. Rigler and U. Mets, *SPIE Proc.-Soc. Int. Opt. Eng.*, 1992, **1921**, 239.
- 16 A. J. de Mello and E. K. Hill, *Analyst*, 2000, **125**, 1033.
- 17 K. Sato, M. Tokeshi, T. Odake, H. Kimura, T. Ooi, M. Nakao and T. Kitamori, *Anal. Chem.*, 2000, **72**, 1144.
- 18 S. C. Jakeway, A. J. de Mello and E. L. Russell, *Fresenius J. Anal. Chem.*, 2000, **366**, 525.
- 19 D. Figeys and D. Pinto, *Anal. Chem.*, 2000, **71**, 330A.
- 20 D. Meldrum, *Genome Research*, 2000, **10**, 1288.
- 21 B. B. Haab and R. A. Mathies, *Anal. Chem.*, 1999, **71**, 5137.
- 22 C. S. Effenhauser, G. J. M. Bruin, A. Paulus and M. Ehrat, *Anal. Chem.*, 1997, **69**, 3451.
- 23 R. Rigler, *J. Biotechnol.*, 2001, **86**, 161.
- 24 M. Gösch, H. Blom, J. Holm, T. Heino and R. Rigler, *Anal. Chem.*, 2000, **72**, 3260.
- 25 D. C. Duffy, J. C. McDonald, O. J. A. Schueller and G. M. Whitesides, *Anal. Chem.*, 1998, **70**, 4974.
- 26 D. Magde, W. W. Webb and E. L. Elson, *Biopolymers*, 1978, **17**, 361.
- 27 R. L. Affleck, W. P. Ambrose, J. N. Demas, P. M. Goodwin, J. A. Schecker, M. Wu and R. A. Keller, *Anal. Chem.*, 1996, **68**, 2270.
- 28 M. S. Osborne, S. Balasubramanian, W. S. Furey and D. Klenerman, *J. Phys. Chem.*, 1998, **102**, 3160.
- 29 Y. Chen, J. D. Müller, P. T. C. So and E. Gratton, *Biophys. J.*, 1999, **77**, 553.
- 30 E. K. Hill and A. J. de Mello, unpublished results, 2000.